Impact of temperature on calendar ageing of Lithium-ion battery using incremental capacity analysis

Matthieu Maures, Yuanci Zhang, Cyril Martin, Jean-Yves Deletage, Jean-Michel Vinassa, Olivier Briat

Version of Record: https://www.sciencedirect.com/science/article/pii/S0026271419304731
Manuscript_90a82f420290748c988901dae139f3dc

Impact of temperature on calendar ageing of Lithium-ion battery using incremental capacity analysis

M. Maures[a,*], Y. Zhang[a], C. Martin[a], J.-Y. Delétage[a], J.-M. Vinassa[a], O. Briat[a]

[a] *Univ. Bordeaux, CNRS Bordeaux INP, IMS, UMR 5218, F-33400 Talence, France*

Abstract

In this paper, a calendar ageing model featuring time and temperature dependence of a Lithium-ion battery is proposed. The ageing procedure is done at a high state of charge (SoC) of 95% and the tested temperatures range from -20°C to 55°C. Electrochemical methods such as incremental capacity analysis (ICA) and differential voltage analysis (DVA) are used to quantify the evolution of the most important degradation modes such as conductivity loss (CL), loss of active material (LAM) and loss of lithium inventory (LLI). While the quantification methods used here are extracted from previous power cycling studies, their validity on calendar ageing data is verified, and a model of each degradation mode evolution versus time including temperature parametrization is proposed.

1. Introduction

Since the emergence of electric vehicles (EVs) to answer the negative effects of CO_2 emissions on climate change and global warming, the Lithium-ion battery market has tripled, and the EV market is set to reach up to 60% of the car market by 2050 [1,2]. Meanwhile, more electric aircrafts (MEAs) are also increasingly using batteries to power their on-board systems and regulate the voltage demand [3].

However, multiple drawbacks remain with this technology and prevent its early adoption in those applications. In particular, EVs present range, charging time and lifespan (of the battery packs) issues compared to internal combustion engine (ICEs) vehicles. MEAs on the other hand face significant challenges regarding the safety and the state of health (SoH) of their batteries, since they can face important temperature variations from -20°C to 55°C.

The SoH of a battery indicates how close it is to its end of life, when a specific failure criterion is met. Depending on energy and power requirements of the target application, the SoH can be defined as SoH_E and SoH_P respectively [4,5]. The SoH_E corresponds to the ratio of the current maximal capacity over the initial maximal capacity, while the SoH_P corresponds to the rise in internal resistance of the battery, which is correlated to more Joule losses hence less usable power for the application. Both SoH are affected by the chemistry of the cell, the temperature and the current draw.

To quantify and model the SoH and its dependence on the batteries' working conditions, ageing tests must be performed. Usually, those can be done in several ways: abuse test, power cycling, and calendar ageing.

Abuse tests are described in [6] and consist in tests that are outside of the manufacturer recommended specifications. Power cycling can be done with an idealized current profile, at a given ambient temperature and C-rate [5,7], or based on the repetition of a current profile which is representative of the application. The C-rate is a current unit based on the capacity of the cell and the desired time of discharge. For example, a 1C current will discharge the battery in 1h, while a C/20 current will discharge it in 20h.

Finally, calendar ageing consists in studying the battery degradation when it is not under load. Degradations of the battery are often described as combination of cycling and calendar ageing. Extensive work on calendar ageing has been made by [9,10] at temperatures above 25°C and 40°C respectively, while [11] studied the effect of calendar ageing on supercapacitors. Ref. [12] studied the identification of calendar degradation through ICA, although did not provide quantification of the different degradation modes that can be observed.

In this paper, the quantification of the evolution of three degradation modes is presented. As this was already performed on cycling tests at 25°C by [5], a

* Corresponding author. matthieu.maures@u-bordeaux.fr
Tel: +33 (5) 40 00 26 58

key contribution here is to test it during calendar ageing, and over a large temperature range. Since the Arrhenius law usually describes the effect of temperature on degradation mechanisms, its validity as an acceleration factor of degradation modes is also tested, and an alternative is proposed.

This paper is divided as following: firstly, a reminder of the different degradation modes occurring in lithium-ion batteries, and the formulation of their quantifications based on literature models and incremental capacity and differential voltage analysis (ICA and DVA respectively) are presented. Secondly, the experimental protocol and the associated results of the calendar ageing are shown. Thirdly, a temperature study of the degradation modes and the validity of the Arrhenius law is questioned. Finally, the conclusion is drawn.

2. Degradation evolutions formulations

The degradation of batteries can be summarized in four categories: causes, degradation mechanisms, degradation modes and effects on the battery [13].

Since degradation mechanisms are numerous and attributed to internal parasitic chemical reactions, it can be tricky to quantify each of them without opening the battery. They can however be grouped in three distinct degradation modes [5]: conductivity loss (CL), caused by the cracking and the dissolution of the current collectors and their binder, loss of active material (LAM), which results from the consumption of electrode material in chemical side reactions, and loss of lithium inventory (LLI), when the Lithium reacts with the electrolyte to form solid electrolyte interphase (SEI), or when, at lower temperatures, lithium plating of the negative electrode occurs.

Previous work [5,14] showed it is possible to quantify the relative evolution of each degradation mode using incremental capacity analysis (ICA) and differential voltage analysis (DVA). Each method consists in performing a charge or a discharge with specific conditions then deriving the capacity (ICA) or the voltage (DVA) and plotting it versus the voltage (ICA) or the capacity (DVA). This usually leads to peaks and valleys (as seen in Fig. 1.). These analyses can be done on characterization curves (check-ups) performed regularly during an accelerated ageing test.

From there, three formulas can be extracted to quantify those evolutions [8]:

$$G_{CL} = \frac{\max(OCV)_1 - \max(OCV)_n}{\max(OCV)_1} \qquad (1)$$

$$G_{LAM} = \frac{\left|\max\left(\frac{dQ}{dV}\right)\right|_1 - \left|\max\left(\frac{dQ}{dV}\right)\right|_n}{\left|\max\left(\frac{dQ}{dV}\right)\right|_1} \qquad (2)$$

$$G_{LLI} = \frac{|\max(Q)|_1 - |\max(Q)|_n}{|\max(Q)|_1} \qquad (3)$$

where:

- G_{CL} is the relative evolution of the degradation through conductivity loss,
- G_{LAM} is the relative evolution of the degradation through loss of active material of the entire battery,
- G_{LLI} is the relative evolution of the degradation through loss of lithium inventory,
- OCV (V) is the battery open circuit voltage,
- Q (Ah) is the capacity of the battery. In this paper, the discharged capacity will be used,
- V (V) is the voltage of the battery,
- n is the index of the check-up at which the quantification of degradations is made.

3. Experimentations

To compute each degradation growth from ICA and DVA, ageing tests were performed.

3.1 Protocol of experiments

All the tests were performed at the Cacyssée platform at the IMS laboratory. This platform is designed to conduct different types of tests on storage devices such as supercapacitors or Lithium-ion batteries. The platform includes several climatic chambers as well as numerous electrochemical stations and measurement devices that are used to perform impedance spectroscopies, power and thermal cycling, or calendar ageing of the storage systems.

Here, six Samsung INR18650-25R5 Lithium-ion batteries were used in this protocol. They feature Nickel-Cobalt-Aluminum (NCA) cathodes and Graphite anodes, and a commercial capacity of 2500mAh. The batteries were held in place using BioLogic BH-1i holders and placed inside Climats EX5413TA climatic chambers.

The temperatures were recorded using Type K thermocouples taped onto the surface of the batteries. Electrical measurements were performed using the four-wires method, connected to a BioLogic BCS-815 device remotely programmed on a computer through the EC-Lab software. Data points were measured every 30 seconds or every 10mV voltage variation.

The ageing procedure can be summarized in the Table 1 below.

Table 1.
Calendar ageing procedure.

Step	Procedure
1	Initial Check-up (see Fig. 1. below).
2	The battery SoC is set to 95%.
3	The battery is put to test temperature.
4	Calendar ageing for a set amount of time.
5	Test stops. The battery waits for 4h at $T_{amb} \approx 24°C$.
6	Check-up (same procedure as in step 1).
7	Repeat steps 2 to 7 until the battery dies.

Unless specified, all charges/discharges are 1C CCCV/1C CC respectively. This means charges are separated in two phases: a constant current phase (CC) until it reaches a given voltage (here 4.2V), then a constant voltage phase (CV), where the current drawn by the battery will slowly decrease until it reaches an end criterion (a C/20 current here). Discharges on the other end never feature a CV phase. Each check-up (see Fig. 1. below, where the circled numbers refer to the procedures described hereafter) consists of a charge ① from 95% (or 50% for the initial check-up, as newly received fresh batteries usually have a ~50% initial SoC) to 100% SoC, 30min of OCV ②.

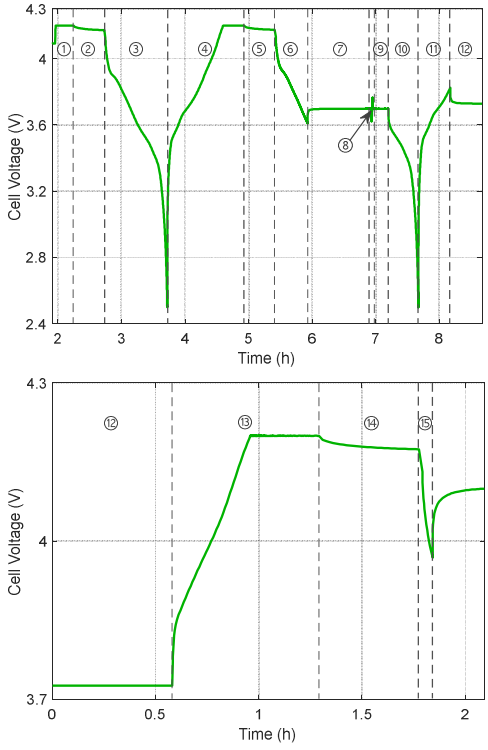

Fig. 1. Check-up (top) and 95% SoC set-up procedures (bottom).

Then, a full discharge/charge ③/④ to measure the capacity, 30min of OCV ⑤, a discharge ⑥ until the battery reach 3.6V (its nominal voltage) and 1h of OCV ⑦. A resistance measurement ⑧ using ±1C 30s pulses is then done. After 15min of OCV ⑨, the battery is fully discharged ⑩ then charged ⑪ for 30min (no CV phase here). The battery then rests for a few hours ⑫ until they are charged back ⑬ to 100% SoC, relax for 30min ⑭, then discharge ⑮ for 3min (~5% of the capacity). This procedure provides a lot of information although, in this paper, all of the information is extracted from the discharge only.

After the initial check-up, the batteries are labelled based on their ageing temperature. Two batteries are chosen for each temperature to ensure repeatability. The characteristics of the batteries are summed-up in Table 2 below.

It should be noted that, for different temperatures, not all check-ups were done at the same time. Since it was initially assumed batteries would age the slowest at 25°C, check-ups on SA09 and SA10 were performed every 1000h on average, while they were performed every 500h on average on the others.

Table 2.
Batteries characteristics and test conditions.

Label	Initial Capacity (mAh)	Test Temperature (°C)
SA09	2508.41	25
SA10	2499.28	25
SA17	2483.94	-20
SA18	2459.35	-20
SA21	2463.03	55
SA22	2454.83	55

3.2 Experimental results

In order to calculate the evolution of each degradation mode, discharge, IC, and DV curves are required. First, the voltage and capacity values of the batteries operating at the same temperature are averaged together. Then, the IC and DV curves are computed in MATLAB using the "diff" function. To avoid parasitic peaks and quantification noise, both the voltage and the capacity are filtered using a Fourier transform and a numerical low-pass filter. Those operations result in the three set of curves

represented in Fig. 2. To improve readability, only curves averaged on SA09 and SA10 are presented. In this case relatively monotonous behaviours with respect to ageing time can be seen, although this is not necessarily the case at other temperatures, as explained in part 4.

It should also be noted that the computation of LAM degradation using equation (2) is peak sensitive. In particular, each peak in the IC curve represents a chemical reaction, more specifically a phase transition of an electrode active material [16]. In our case, the peak around 3.55V is used to compute LAM. As it can be seen in Fig. 2 and Fig. 3, the peak position does not move significantly with ageing temperature. This is on par with previous work [5,12] where this peak is used for SoH estimation.

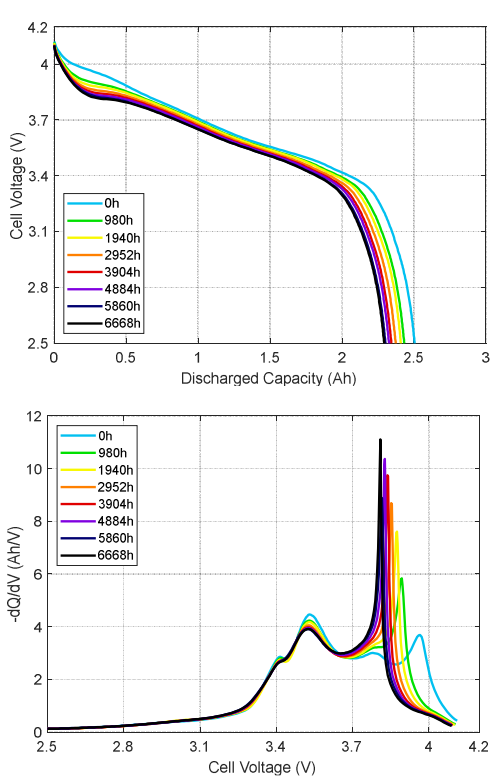

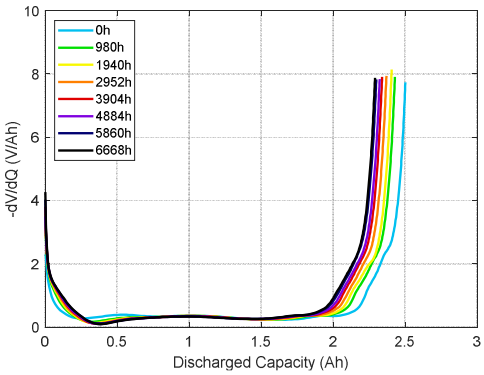

Fig. 2. Discharge curves (top), IC curves (middle) and DV curves (bottom) averaged on SA09 and SA10 at 25°C, for multiple calendar ageing times.

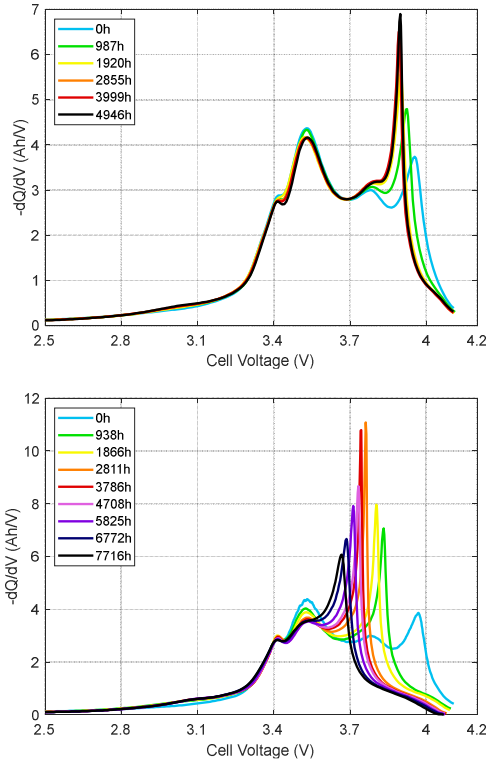

Fig. 3. IC curves for calendar ageing done at -20°C (top) and 55°C (bottom).

4. Time and temperature models of degradations

4.1 Degradation evolutions time dependence

After calculating degradation evolutions using equations (1), (2) and (3), and plotting them against the square root of the calendar ageing time, linear behaviours can be seen (see Fig. 4.). In particular, squared correlation coefficients for each degradation

and temperature are shown in Table 3.

They are relatively high (often higher than 0.85), except at -20°C, particularly for the CL degradation mode. Multiple factors can explain this: first, no break-in has been performed on the batteries.

Usually, break-in consists in fully charging/discharging the batteries three times, using C/2 CCCV/C/2 CC procedures respectively, and leads to increase in capacity of the battery. In our case, this leads to dips (sometimes negative) in the first values, which wouldn't happen otherwise.

Furthermore, the computation of the CL degradation evolution is normally based on pseudo-OCV values (voltage values from low C-rate discharges, below C/10). Here, check-ups are performed at 1C. To compute G_{CL}, the voltage at the end of the first relaxation period is used. This value however is close enough from its pseudo-OCV counterpart [16] to justify its use here.

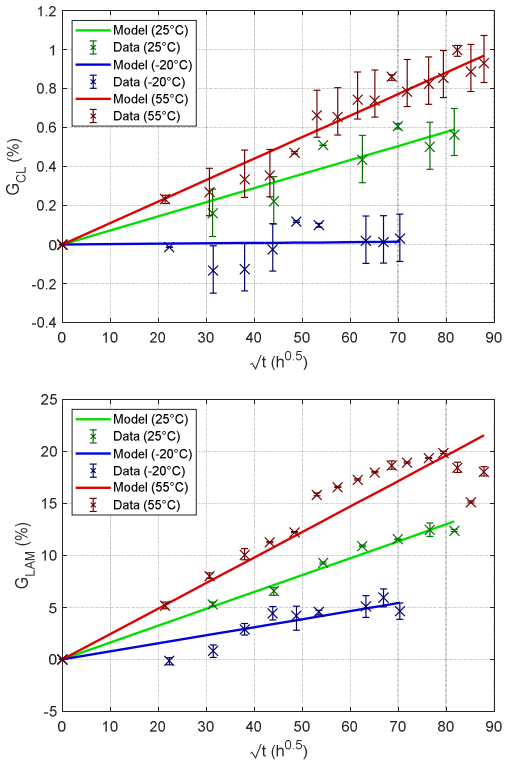

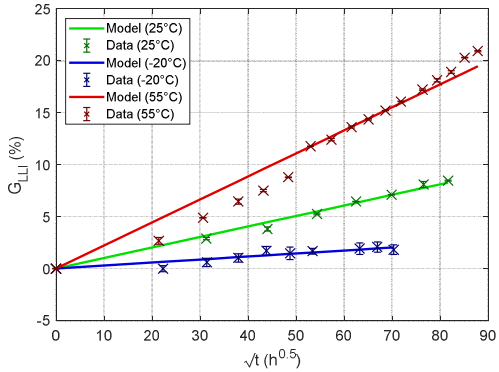

Fig. 4. Growths of CL (top), LAM (middle) and LLI (bottom) against the square root of time.

CL growth also features relatively important error bars, indicating it is explained that improvements in battery manufacturing processes limit this degradation.

Table 3.
R^2 between linear models and data points.

T (°C)	25°C	-20°C	55°C
R^2_{CL}	0.88	0.016	0.95
R^2_{LAM}	0.98	0.80	0.85
R^2_{LLI}	0.99	0.85	0.96

4.2 Temperature parametrization

For each degradation, the linear model can be written as:

$$G = A\sqrt{t} \qquad (4)$$

where logarithms of A_{CL}, A_{LAM}, and A_{LLI} can all be plotted against the inverse temperature. As seen in Fig. 5. below, LAM and LLI coefficients can be modelized by an Arrhenius law, hence:

$$G = G_0 e^{-\frac{E_a}{k_B T}}\sqrt{t} \qquad (5)$$

where k_B is the Boltzmann constant, and the G_0 parameters and E_a activation energies are summed-up in the Table 4 below. This is interesting since, usually, the Arrhenius law serves as a degradation mechanism model. Degradation modes are a composition of multiple mechanisms with different properties that do not necessarily add up into another Arrhenius model. Mathematically, this can be explained if a degradation mechanism predominates the others. This is also supported by [10] where

similar equations can be found to directly model the capacity fade, but at higher temperatures (between 40°C and 60°C). There, the capacity fade is assumed to be directly correlated to LLI, which is itself associated with SEI formation and follows an Arrhenius law. However, at lower temperatures, SEI formation is not necessarily the predominant degradation mechanism, in particular at -20°C where lithium plating occurs, yet Fig. 5 suggests the Arrhenius law remains valid nonetheless.

Meanwhile, on the same figure, the CL mode presents worse linearity than the others ($R^2 = 0.942$, compared to 0.999 for LAM and 0.997 for LLI), however, when plotting A_{CL} against the inverse temperature (see Fig. 5), the linearity is improved significantly ($R^2 > 0.999$), and can be described by the following proposed model:

$$G = G_0 \left(1 - \frac{E_a}{k_B T}\right) \sqrt{t} \qquad (6)$$

This formalism was chosen to allow comparison between the two different model, where the G_0 and E_a parameters in (6) are presented in the Table 4 below.

Table 4.
Model parameters for each degradation.

	CL (6)	LAM (5)	LLI (5)
G_0 (%/h$^{0.5}$)	0.0474	11.7	189
Ea (zJ)	3.48	17.5	30.7

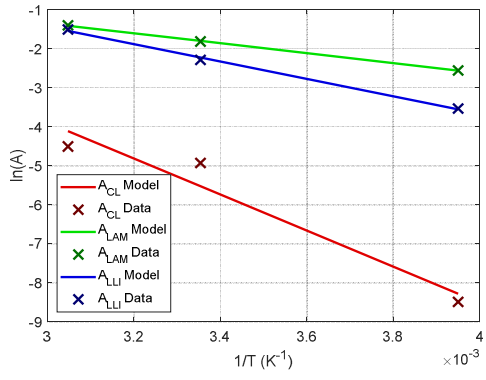

Fig. 5. Arrhenius law of the linear coefficient between each degradation and the square root of the time. This model does not seem suitable for the CL mode.

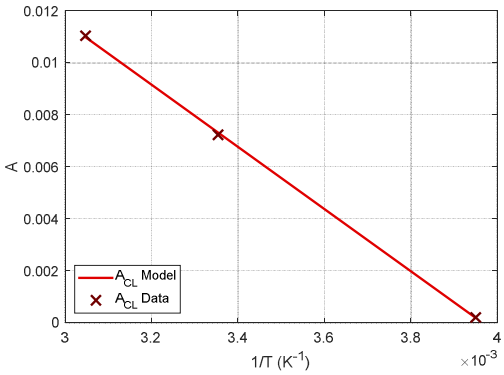

Fig. 6. New model of the linear coefficient between the CL degradation mode and the square root of the time.

Conclusion

An extension to temperature-dependent ageing models was presented. Three degradation modes known as conductivity loss, loss of active material, and loss of lithium inventory were chosen, and, based on previous work, their identification and quantification through ICA and DVA was shown. Although the formulations of the degradation modes evolutions were extracted from power cycling literature tests, they were proven to be adequate for calendar ageing tests. An ageing model of each degradation mode featuring temperature parametrization was then presented, and although the Arrhenius law proved to be sufficient for accurate representation of the LAM and LLI degradation modes, a new simple model was proposed for the CL.

This model could be improved by performing a new ageing test with more data points in order to increase the correlation between the degradation growth and the square root of time. The new test could also use more batteries to check statistical variations.

Future work should seek for a correlation between each of these degradation modes and their main effects: capacity loss and power fade. This would be especially useful to create an ageing model of the internal resistance of the battery, which is heavily correlated to the CL degradation mode.

References

[1] C. Pillot, aabc Europe, 2017.

[2] T. Gnann, T. S. Stephens, Z. Lin, P. Plötz, C. Liu, and J. Brokate, *Renewable and Sustainable Energy Reviews*, vol. 93, pp. 158–164, May 2018.

[3] R. Mishra and R. Saxena, *2017 7th International Conference on Power Systems, ICPS 2017*, pp.

702–707, 2018.
[4] D. Andre, C. Appel, T. Soczka-Guth, and D. U. Sauer, *Journal of Power Sources*, vol. 224, pp. 20–27, 2013.
[5] C. Pastor-Fernández, W. D. Widanage, G. H. Chouchelamane, and J. Marco, *6th Hybrid and Electric Vehicles Conference (HEVC 2016)*, 2016.
[6] V. Ruiz, A. Pfrang, A. Kriston, N. Omar, P. Van den Bossche, and L. Boon-Brett, *Renewable and Sustainable Energy Reviews*, vol. 81, May 2017, pp. 1427–1452, 2018.
[7] C. R. Birkl *et al.*, *Journal of The Electrochemical Society*, vol. 164, no. 12, pp. A2644–A2653, 2017.
[8] C. Pastor-Fernández, K. Uddin, G. H. Chouchelamane, W. D. Widanage, and J. Marco, *Journal of Power Sources*, vol. 360, pp. 301–318, 2017.
[9] A. Eddahech, O. Briat, E. Woirgard, and J. M. Vinassa, *Microelectronics Reliability*, vol. 52, no. 9–10, pp. 2438–2442, 2012.
[10] S. L. Hahn, B. Obry, M. Storch, R. Swaminathan, K. P. Birke, and J. Bandlow, *Journal of Power Sources*, vol. 400, pp. 402–414, July 2018.
[11] O. Briat, J. M. Vinassa, N. Bertrand, H. El Brouji, J. Y. Delétage, and E. Woirgard, *Microelectronics Reliability*, vol. 50, no. 9–11, pp. 1796–1803, 2010.
[12] Y. C. Zhang, O. Briat, J. Y. Delétage, C. Martin, N. Chadourne, and J. M. Vinassa, *Microelectronics Reliability*, vol. 88–90, pp. 1231–1235, July 2018.
[13] C. R. Birkl, M. R. Roberts, E. McTurk, P. G. Bruce, and D. A. Howey, *Journal of Power Sources*, vol. 341, pp. 373–386, 2017.
[14] M. Dubarry, C. Truchot, and B. Y. Liaw, *Journal of Power Sources*, vol. 219, pp. 204–216, 2012.
[15] M. Dubarry *et al.*, *Journal of Power Sources*, vol. 196, no. 23, pp. 10328–10335, 2011.
[16] P. Keil and A. Jossen, *Journal of Energy Storage*, vol. 6, pp. 125–141, 2016.